

Magnetotransport in copper-doped noncentrosymmetric BiTeI

Chang-Ran Wang,¹ Jen-Chuan Tung,² R. Sankar,³ Chia-Tso Hsieh,¹ Yung-Yu Chien,¹
Guang-Yu Guo,^{2,4,*} F. C. Chou,³ and Wei-Li Lee^{1,†}

¹*Institute of Physics, Academia Sinica, Nankang, Taipei 11529, Taiwan*

²*Graduate Institute of Applied Physics, National Chengchi University, Taipei 11605, Taiwan*

³*Center for Condensed Matter Sciences, National Taiwan University, Taipei 10617, Taiwan*

⁴*Department of Physics and Center for Theoretical Sciences, National Taiwan University, Taipei 10617, Taiwan*

(Received 4 March 2013; revised manuscript received 3 July 2013; published 9 August 2013)

BiTeI exhibits large Rashba spin splitting due to its noncentrosymmetric crystal structure. The study of the chemical doping effect is important in order to either tune the Fermi level or refine the crystal quality. Here, we report the magnetotransport measurement in high quality BiTeI single crystals with different copper dopings. We found that a small amount of copper doping improves the crystal quality significantly, which is supported by the transport data showing higher Hall mobility and larger amplitude in Shubnikov–de Haas oscillation at low temperature. Two distinct frequencies in Shubnikov–de Haas oscillation were observed, giving extremal Fermi surface areas of $A_S = 9.1 \times 10^{12} \text{ cm}^{-2}$ and $A_L = 3.47 \times 10^{14} \text{ cm}^{-2}$ with corresponding cyclotron masses $m_S^* = 0.0353m_e$ and $m_L^* = 0.178m_e$, respectively. Those results are further compared with relativistic band structure calculations using three reported Te and I positions. Our analysis infers the crucial role of Bi-Te bond length in the observed large bulk Rashba-type spin-splitting effect in BiTeI.

DOI: [10.1103/PhysRevB.88.081104](https://doi.org/10.1103/PhysRevB.88.081104)

PACS number(s): 71.18.+y, 71.15.-m, 73.43.Qt, 75.70.Tj

BiTeI emerges as an intriguing material that shows a large Rashba effect^{1–3} and a possible topological phase transition under pressure.⁴ Its crystal structure comprises alternating layers of bismuth (Bi), tellurium (Te), and iodine (I), each with a trigonal planar lattice, as illustrated in Fig. 1(a). It was proposed⁵ to constitute a semi-ionic structure along the stacking direction, where the (BiTe)⁺ layer is positively charged and the (Bi-I) layer is ionic. Angle-resolved photoemission spectroscopy experiments (ARPES)^{1,6} have revealed evidence for the giant Rashba spin splitting, and its bulk nature was further confirmed by bulk-sensitive optical spectroscopy⁷ and soft x-ray ARPES.⁸ When comparing to the band structure calculation, the Te and I coordinations turn out to be crucial parameters that can result in a dramatic difference in the calculated band property. There are three different Te and I coordinations reported in the literature: coordination A with Te(2/3, 1/3, 0.6928) and I(1/3, 2/3, 0.2510) from the refinement analysis of x-ray experiment,⁵ as well as coordination B with Te(2/3, 1/3, 0.7111) and I(1/3, 2/3, 0.2609),⁹ and coordination C with Te(2/3, 1/3, 0.7482) and I(1/3, 2/3, 0.3076),¹⁰ from two different theoretical structural determinations using the same band structure method. Regardless of the small variation, only coordination C with a shortest Bi-Te bond length ($d_{\text{Bi-Te}} = 3.05 \text{ \AA}$) gives rise to a giant Rashba spin splitting in the bulk band with a Rashba parameter $\alpha_R \cong 5.4 \text{ eV \AA}$ according to our calculations, which may infer a close connection between $d_{\text{Bi-Te}}$ and its Rashba effect.

In this Rapid Communication, we show magnetotransport measurement results on high quality Cu_xBiTeI single crystals with copper (Cu) doping x up to 0.2. Comparing to earlier works on Shubnikov–de Haas (SdH) oscillations,^{11,12} the SdH oscillation in our crystals exhibits two distinct frequencies derived from a large Fermi surface (LFS) and a small Fermi surface (SFS), which is an order of magnitude larger in amplitude at similar temperatures. The corresponding Fermi surface areas and cyclotron masses can then be

unambiguously determined and compared to relativistic band structure calculations using three different atomic coordinations A, B, and C with progressive reduction in $d_{\text{Bi-Te(I)}}$. Our experimental results, including the angular dependence of SdH frequencies, are in good agreement with the calculation using coordination C and thus provide a strong evidence for the bulk nature of the large Rashba spin-splitting effect.

Single crystals of BiTeI were grown by direct mixing of pristine elements of Bi, Te, and I with an additional room temperature agglomeration procedure.¹³ The powder x-ray diffraction patterns of ground BiTeI crystals with Cu content $x = 0, 0.075, \text{ and } 0.1$ are shown in Fig. 1(b), where the lattice parameters were determined using space group $P3m1$ to be $a = b = 4.3421 \text{ \AA}$ and $c = 6.8835 \text{ \AA}$ for the pristine sample of $x = 0$. As x increases, the lattice expands more along the stacking direction, as shown in the inset of Fig. 1(b). The in-plane resistivity ρ shown in Fig. 1(c) exhibits metallic behavior down to 5 K, below which it becomes nearly temperature independent. The carrier density n_e and Hall mobility μ_H were obtained from the Hall effect measurement and shown in the upper inset of Fig. 1(c). It is quite evident that the addition of Cu effectively reduces the electron concentration in BiTeI and improves the carrier mobility by nearly an order of magnitude, where SdH oscillation appears with a large amplitude and enables the extraction of the band parameters to be compared with relativistic band calculations.

The upper inset of the Fig. 2 shows the magnetoresistance (MR) $[\rho(H)/\rho(0)] - 1$ for $x = 0, 0.075, \text{ and } 0.1$ as a function of magnetic field up to 15 T at $T = 5 \text{ K}$. It exhibits positive MR and starts to show SdH oscillations above 3 T. The pure oscillatory component $\Delta\rho$ in the resistivity¹⁴ is extracted and plotted as a function of $1/\mu_0 H$, as shown in Fig. 2. We remark that the oscillation amplitude is at least threefold larger comparing to the undoped for samples with $x = 0.075$ and 0.1 as shown in the red and blue lines, respectively. By taking the fast Fourier transformation (FFT) of the MR data, two apparent

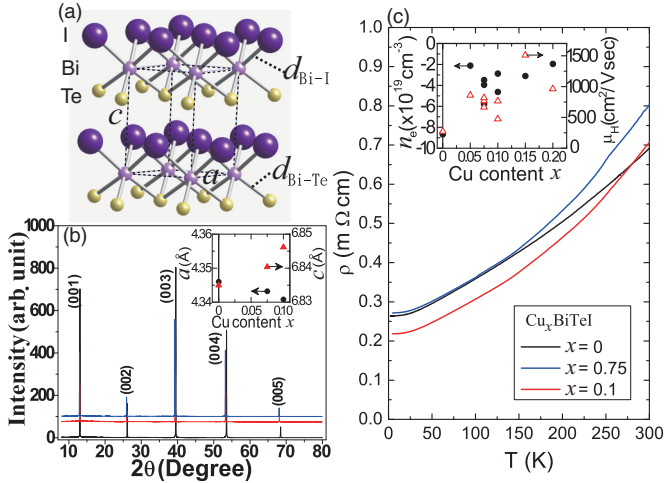


FIG. 1. (Color online) (a) An illustration of the BiTeI crystal structure. $d_{\text{Bi-Te(I)}}$ is the Bi-Te(I) bond length. (b) shows the powder x-ray diffraction pattern of ground Cu_xBiTeI single crystals with $x = 0, 0.075,$ and 0.1 . The inset figure shows the x dependence on the lattice constants a and c . (c) The resistivity $\rho(T)$ for $x = 0, 0.075,$ and 0.1 crystals. The upper inset plots the carrier density n_e (solid circle) and the corresponding Hall mobility μ_H (open triangle) at 5 K vs Cu content x .

peaks at F_S and F_L for $x = 0.075$ and 0.1 were identified in the FFT spectrum shown in the lower inset of Fig. 2, where the suffixes S and L are referred as deriving from a SFS and a LFS, respectively.

According to the Lifshitz-Kosevich (LK) formalism, $\Delta\rho$ can be expressed as

$$\Delta\rho(T, B) = \exp[-X(T, B)] \frac{X(T, B)}{\sinh[X(T, B)]} \Delta\rho', \quad (1)$$

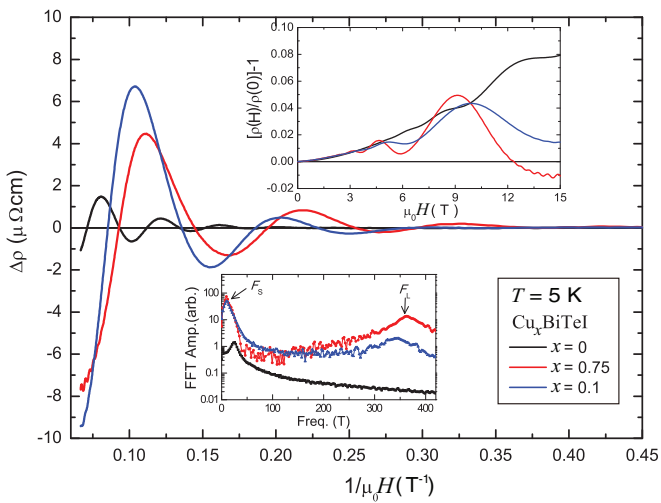


FIG. 2. (Color online) The oscillatory component of the resistivity $\Delta\rho$ as a function of $1/\mu_0 H$ at 5 K for $x = 0, 0.075,$ and 0.1 crystals. The upper inset shows the magnetoresistance before subtracting the nonoscillatory component of the resistivity. The corresponding FFT spectrum is shown in the lower inset, where two local extremes at F_S and F_L can be clearly identified.

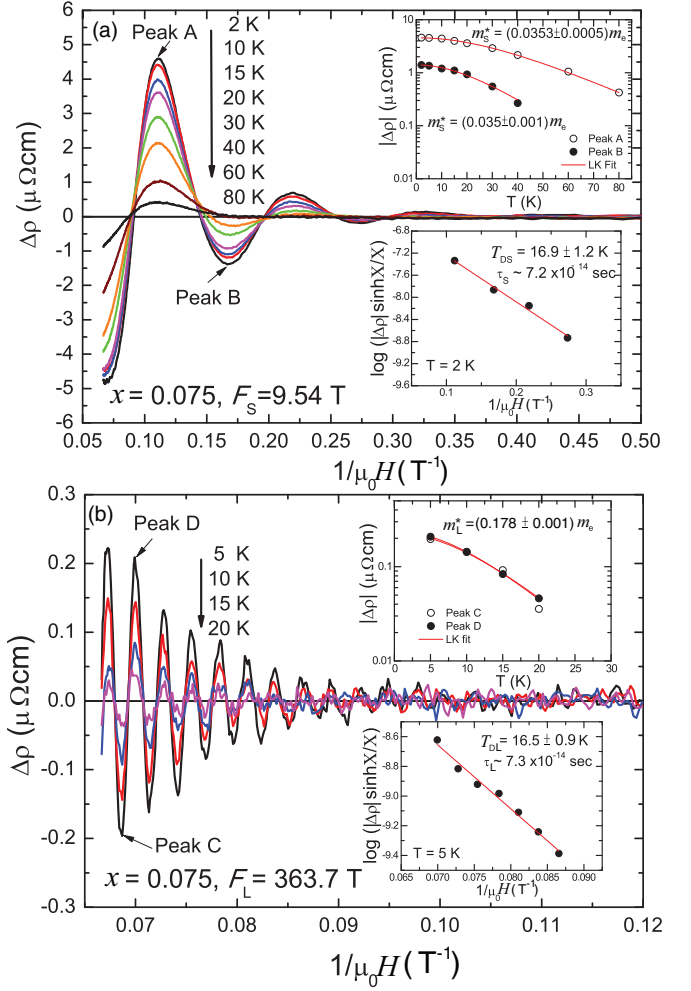


FIG. 3. (Color online) (a) SdH oscillations of SFS at eight different temperatures up to 80 K. The temperature dependence of amplitude $|\Delta\rho|$ at peak A (open circle) and peak B (solid circle) are shown in the upper inset. The red lines are fitting curves using the LK formula for effective cyclotron mass m^* determination. The lower inset shows the linear fit to $\log(|\Delta\rho| \sinh X/X)$ at local peaks vs $1/\mu_0 H$, where the Dingle temperature T_D can be calculated from the slope. Similarly, (b) shows the SdH oscillations of LFS at four different temperatures. The m^* and T_D are determined via the LK formula fitting, as shown in the upper inset and lower inset, respectively.

where $\Delta\rho'$ refers to the oscillatory component without damping, $X(T, B) \equiv 2\pi^2 k_B T m^* / \hbar e B$, m^* is the effective cyclotron mass, and T_D is the Dingle temperature. Figure 3(a) and 3(b) show the oscillatory component $\Delta\rho$ as a function of $1/\mu_0 H$ at different temperatures in the $x = 0.075$ sample arising from SFS and LFS, respectively. In Fig. 3(a), the SdH frequency F_S equals 9.54 T with an oscillation amplitude as large as $5 \mu\Omega \text{ cm}$ at 2 K, where it remains observable with temperatures as high as 80 K. By fitting the temperature dependence of $\Delta\rho$ with the LK formula shown in the upper inset in Fig. 3(a), we obtained consistent effective cyclotron masses $m_S^* = 0.0353 \pm 0.0005 m_e$ and $0.035 \pm 0.001 m_e$ for peak A and peak B locations, respectively, where m_e is the electron rest mass. For T_{DS} determination, we plot $\log(|\Delta\rho| \sinh X/X)$ at local extremes as a function of their corresponding $1/\mu_0 H$,

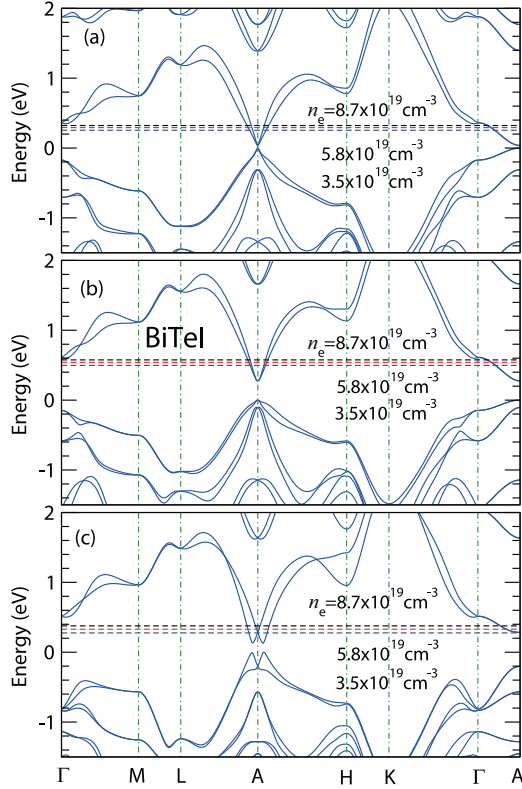


FIG. 4. (Color online) Relativistic band structure of BiTeI in the trigonal $P3m1$ structure using (a) coordination A from Ref. 5 and as well as the theoretically determined (b) coordination B (Ref. 9) and (c) coordination C (Ref. 18). The top of the valence band is at 0 eV. The lower, middle, and upper dashed horizontal lines denote the Fermi level for electron concentrations $n_e = 3.5, 5.8,$ and $8.7 (\times 10^{19} \text{ cm}^{-3})$, respectively.

as demonstrated in the lower inset of Fig. 3(a). The data points can be linearly fitted based on the LK formula, giving a $T_{DS} = 16.9 \pm 1.2$ K, which corresponds to an electron scattering lifetime $\tau_S \equiv \hbar/2\pi k_B T_{DS} \cong 7.2 \times 10^{-14}$ s. On the other hand, Fig. 3(b) shows the SdH oscillation arising from LFS, giving a $F_L = 363.7$ T. The effective cyclotron mass m_L^* equals $0.178 \pm 0.001 m_e$ from the LK fitting using either peak C or D, as shown in the upper inset of Fig. 3(b). The T_{DL} is about 16.5 ± 0.9 K, giving a $\tau_L \cong 7.3 \times 10^{-14}$ s. The extremal Fermi surface area A_e perpendicular to the field direction can be deduced from the SdH oscillation frequency via the Onsager formula $F = \frac{\hbar}{2\pi e} A_e$, which gives $A_S = 9.1 \times 10^{12} \text{ cm}^{-2}$ and $A_L = 3.47 \times 10^{14} \text{ cm}^{-2}$ for SFS and LFS, respectively.

To gain insight into our magnetotransport experiments, we perform relativistic band structure calculations for BiTeI within the density functional theory with the generalized gradient approximation (GGA)¹⁵ by using the accurate projector augmented-wave (PAW) method, as implemented in the VASP package.^{16,17} All three coordinations A,⁵ B,⁹ and C (Ref. 18) were considered. A large plane-wave cutoff energy of 250 eV was used. The calculated band structures are shown in Fig. 4, where three horizontal dashed lines in black, red, and blue denote the Fermi level for electron density $n_e = 8.7, 5.8,$ and $3.5 (\times 10^{19} \text{ cm}^{-3})$, respectively, which were set based on the experimental electron densities in crystals of $x = 0, 0.075,$

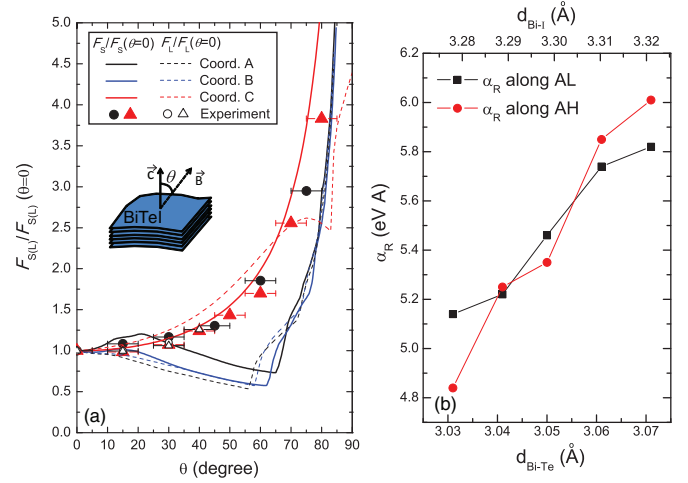


FIG. 5. (Color online) (a) Relative SdH oscillation frequency $F_{S(L)}/F_{S(L)}(\theta=0)$ as a function of θ for two $x = 0.075$ crystals are shown as solid (open) symbols. θ is defined as the angle between the BiTeI stacking direction \vec{c} and magnetic field direction \vec{B} , as illustrated in the inset cartoon. The solid (dashed) lines are the calculated $F_{S(L)}/F_{S(L)}(\theta=0)$ using coordination A, B, and C. The experimental data points agree well with the calculated curves using coordination C within the error. (b) Calculated Rashba parameter α_R vs given Bi-Te bond lengths ($d_{\text{Bi-Te}}$) close to that of coordination C.

and 0.1. We remark that large bulk Rashba spin splitting occurs only for coordination C. Using a rigid band assumption, the Cu doping merely decreases the carrier density of the system and hence shifts the Fermi level lower. We found that experimental values of F and m^* at three different carrier densities of $n_e = 3.5, 5.8,$ and $8.7 (\times 10^{19} \text{ cm}^{-3})$ as listed in Table I are much more close to the calculated values using coordination C, which gives the shortest bond length $d_{\text{Bi-Te}} = 3.05$ Å.

We also performed angular dependence measurements of the SdH oscillation for two $x = 0.075$ crystals in the same batch to further identify the shape of the Fermi surface.¹⁴ The normalized SdH frequency $F_{S(L)}/F_{S(L)}(\theta=0)$ as a function of field angle θ is plotted in Fig. 5(a), where the closed (open) symbols and solid (dashed) lines are experimental data and calculated values for SFS (LFS), respectively. The field angle θ is defined as the angle between the stacking direction \vec{c} and external field, as illustrated in the inset cartoon of Fig. 5(a). Even though the SdH frequency differs slightly from sample to sample in the same batch, we remark that the normalized SdH frequency $F_{S(L)}/F_{S(L)}(\theta=0)$ remains to follow well with the calculated band using coordination C, as shown in the circles and triangles in Fig. 5(a). For more than four crystals of $x = 0.075$ in the same batch we measured, $F_S(\theta=0)$ values fall in a range of 3.6–9.54 T with a corresponding electron density in a range of 3.5 – $5.8 \times 10^{19} \text{ cm}^{-3}$. This somewhat large variation in $F_S(\theta=0)$ turns out to have no apparent correlation with n_e ,¹⁴ and thus infers a sizable variation of the α_R even in the same batch of Cu_xBiTeI crystals.

The Cu dopings are most likely achieved through the internal redox reaction of the intercalated Cu in the van der Waals gap. While there is no superlattice observed from both powder x-ray and Laue diffraction results up to about

TABLE I. Comparison of calculated SdH frequency F (T) and effective mass $m^*(m_e)$ using three different coordinations to experimental data. $d_{\text{Bi-Te(I)}} (\text{\AA})$ denotes the Bi-Te(I) bond length. Calculated Rashba parameter $\alpha_R = 0$ for coordinations A and B. For coordination C, $\alpha_R = 5.46$ (5.35) eV \AA along the AL (AH) direction [see Fig. 4(c)].

$n_e(10^{19} \text{ cm}^{-3})$	SdH parameters	3.5		5.8		8.7	
		F (T)	m^* (m_e)	F (T)	m^* (m_e)	F (T)	m^* (m_e)
Coordination A ^a	LFS	175	0.203	247	0.247	317	0.285
	$d_{\text{Bi-Te(I)}} = 3.27$ (3.04) SFS	72.7	0.077	99.5	0.091	125	0.104
Coordination B ^b	LFS	151	0.143	210	0.173	268	0.2
	$d_{\text{Bi-Te(I)}} = 3.19$ (3.08) SFS	104	0.088	140	0.101	173	0.114
Coordination C ^c	LFS	319	0.167	397	0.178	475	0.196
	$d_{\text{Bi-Te(I)}} = 3.05$ (3.30) SFS	0		4.4	0.023	18.8	0.047
Experimental data	LFS	339	0.186	364	0.178		
	SFS	9.2	0.037	9.5	0.035	24.8	0.068

^aTe(2/3, 1/3, 0.6928), I(1/3, 2/3, 0.2510) (Ref. 5).

^bTe(2/3, 1/3, 0.7111), I(1/3, 2/3, 0.2609) (Ref. 9).

^cTe(2/3, 1/3, 0.7458), I(1/3, 2/3, 0.3133) (Ref. 18).

20% Cu intercalation per formula unit, the intercalated Cu should distribute randomly or in various domain sizes within the van der Waals gap. Locally, the induced strain by Cu can be relieved by expanding the lattice along the stacking direction [the inset of Fig. 1(b)] and also by distorting both the $d_{\text{Bi-Te}}$ and $d_{\text{Bi-I}}$ in the same manner. It is then reasonable to describe the various degrees of residue strain of a layered system with an average $d_{\text{Bi-Te}}$ change. By assuming the change of $d_{\text{Bi-I}}$ scales linearly with $d_{\text{Bi-Te}}$ due to Cu intercalation, the calculated α_R values along AL and AH directions can vary as much as 20% (6–4.8 eV \AA) while $d_{\text{Bi-Te(I)}}$ merely drops by 1% (3.07–3.03 \AA), as demonstrated in Fig. 5(b), which suggests a nontrivial role of average $d_{\text{Bi-Te}}$ in the observed Rashba spin-splitting effect. In Table I, both the calculated F and m^* values for coordination C drop monotonically with decreasing electron density n_e while the ratio of $A_L/A_S (=F_L/F_S)$ increases with descending n_e . Apparently, the experimental values in Table I give a smaller F_L/F_S ratio at similar carrier densities that cannot be fully explained by the discrepancy in n_e . We therefore attribute the likely source of deviation to the difference in average $d_{\text{Bi-Te}}$ that dictates α_R . Nevertheless, further investigation is keenly required to show how $d_{\text{Bi-Te(I)}}$ in BiTeI does influence

the charge distribution in the $(\text{BiTe})^+$ layer and hence the Rashba spin-splitting effect.

In conclusion, Cu_xBiTeI is a remarkable system, where we have demonstrated a robust impact of a minor change in atomic coordinations to its band property. The Cu doping not only effectively reduces the electron density but also boosts the carriers' Hall mobility. We observed two distinct frequencies in SdH oscillation, where the corresponding effective cyclotron masses were determined and compared to theoretical band calculations using three different atomic coordinations for Te and I. Our experimental data agree well with the calculation using coordination C with a shortest $d_{\text{Bi-Te}}$, which indicates a close connection between $d_{\text{Bi-Te}}$ and the giant bulk Rashba spin-splitting effect in BiTeI. In principle, α_R can be readily tuned by controlling the BiTeI bond length if applicable. Our finding offers a possibility for engineering the Rashba spin splitting in a layered and noncentrosymmetric material.

The authors acknowledge funding support from National Science Council in Taiwan. W.L.L. acknowledges funding support from Academia Sinica 2012 career development award in Taiwan.

*gyguo@phys.ntu.edu.tw

†wlee@phys.sinica.edu.tw

¹K. Ishizaka, M. S. Bahramy, H. Murakawa, M. Sakano, T. Shimojima, T. Sonobe, K. Koizumi, S. Shin, H. Miyahara, A. Kimura, K. Miyamoto, T. Okuda, H. Namatame, M. Taniguchi, R. Arita, N. Nagaosa, K. Kobayashi, Y. Murakami, R. Kumai, Y. Kaneko, Y. Onose, and Y. Tokura, *Nat. Mater.* **10**, 521 (2011).

²S. V. Ereemeev, I. A. Nechaev, Y. M. Koroteev, P. M. Echenique, and E. V. Chulkov, *Phys. Rev. Lett.* **108**, 246802 (2012).

³M. Sakano, M. S. Bahramy, A. Katayama, T. Shimojima, H. Murakawa, Y. Kaneko, W. Malaeb, S. Shin, K. Ono, H. Kumigashira, R. Arita, N. Nagaosa, H. Y. Hwang, Y. Tokura, and K. Ishizaka, *Phys. Rev. Lett.* **110**, 107204 (2013).

⁴M. S. Bahramy, B. J. Yang, R. Arita, and N. Nagaosa, *Nat. Commun.* **3**, 679 (2011).

⁵A. V. Shevelkov, E. V. Dikarev, R. V. Shpanchenko, and B. A. Popovkin, *J. Solid State Chem.* **114**, 397 (1995).

⁶A. Crepaldi, L. Moreschini, G. Autès, C. Tournier-Colletta, S. Moser, N. Virk, H. Berger, Ph. Bugnon, Y. J. Chang, K. Kern, A. Bostwick, E. Rotenberg, O. V. Yazyev, and M. Grioni, *Phys. Rev. Lett.* **109**, 096803 (2012).

⁷J. S. Lee, G. A. H. Schober, M. S. Bahramy, H. Murakawa, Y. Onose, R. Arita, N. Nagaosa, and Y. Tokura, *Phys. Rev. Lett.* **107**, 117401 (2011).

⁸G. Landolt, S. V. Ereemeev, Y. M. Koroteev, B. Slomski, S. Muff, T. Neupert, M. Kobayashi, V. N. Strocov, T. Schmitt, Z. S. Aliev, M. B. Babanly, I. R. Amiraslanov, E. V. Chulkov,

- J. Osterwalder, and J. H. Dil, *Phys. Rev. Lett.* **109**, 116403 (2012).
- ⁹V. A. Kulbachinskii, V. G. Kytin, A. A. Kudryashov, A. N. Kuznetsov, and A. V. Shevelkov, *J. Solid State Chem.* **193**, 154 (2012).
- ¹⁰M. S. Bahramy, R. Arita, and N. Nagaosa, *Phys. Rev. B* **84**, 041202(R) (2011).
- ¹¹C. Martin, E. D. Mun, H. Berger, V. S. Zapf, and D. B. Tanner, *Phys. Rev. B* **87**, 041104(R) (2013).
- ¹²C. Bell, M. S. Bahramy, H. Murakawa, J. G. Checkelsky, R. Arita, Y. Kaneko, Y. Onose, M. Tokunaga, Y. Kohama, N. Nagaosa, Y. Tokura, and H. Y. Hwang, *Phys. Rev. B* **87**, 081109(R) (2013).
- ¹³R. Sankar, W. L. Lee, and F. C. Chou (unpublished).
- ¹⁴See Supplemental Material at <http://link.aps.org/supplemental/10.1103/PhysRevB.88.081104> for details of the SdH oscillation analysis.
- ¹⁵J. P. Perdew, K. Burke, and M. Ernzerhof, *Phys. Rev. Lett.* **77**, 3865 (1996).
- ¹⁶G. Kresse and J. Hafner, *Phys. Rev. B* **48**, 13115 (1993).
- ¹⁷G. Kresse and J. Furthmüller, *Comput. Mater. Sci.* **6**, 15 (1993).
- ¹⁸We have also determined the Te and I atomic positions theoretically by fully relativistic GGA (Ref. 15) calculations using the PAW method (Refs. 16 and 17). Our theoretical atomic positions of Te(2/3, 1/3, 0.7458) and I(1/3, 2/3, 0.3133) are nearly identical to those reported in Ref. 10 (the bond length differences being within 1.0%).